Construction and Building Materials 444 (2024) 137852

Contents lists available at ScienceDirect

Construction and Building Materials

journal homepage: www.elsevier.com/locate/conbuildmat

Exploring the influence of calcined clay grade on the rheological dynamics of LC^3 mortar

Jiaqi Zhang [a], Qi Luo [a,b,*], Xinyu Zhang [a]

[a] Department of Civil Engineering, Chongqing Jiaotong University, Chongqing 400074, PR China
[b] Department of Civil and Environmental Engineering, National University of, Singapore city 117576, Singapore

ARTICLE INFO

Keywords:
Limestone calcined clay cement (LC^3)
Rheology
Yield stress
Impurity
Metakaolin content

ABSTRACT

This study utilized a synthetic engineering limestone calcined clay (LC^3) system to simulate the effects of different grades of calcined clay on the rheological, hydration, and mechanical properties of LC^3 mortar. By finely grinding quartz to a particle size akin to that of calcined metakaolin and blending it in proportions ranging from 0 % to 100 %, it was able to explore the detailed relationships between metakaolin content and key properties of the mortar. The results show a nonlinear correlation between metakaolin content and rheological behavior, with 85 % metakaolin content identified as the optimal proportion. At this level, the compressive strength values closely approached those of the 100 % group. The result also highlights the significant influence of water to binder ratio and the substitution of wollastonite for limestone on mortar flowability and mechanical strength. Notably, mixes with higher proportions of ground quartz exhibited delayed hydration and reduced early strength but increased long-term strength due to enhanced pozzolanic reactions. A significant contribution of this study is the modification of the traditional rheological formula specifically for LC^3 materials, providing new insights for future research on the rheological properties of LC^3 systems. These findings are crucial for the formulation of more efficient, sustainable LC^3 systems tailored for specific engineering applications. The optimized rheological formula offers a robust foundation for further exploration and refinement of the balance between workability and mechanical performance in LC^3 systems.

1. Introduction

Cement and concrete materials constitute crucial material foundations of modern society and are also among the primary sources of global CO_2 emissions. Statistical data indicates that 70 % of industrial CO_2 emissions worldwide originate from ten major industrialized nations [1], with emissions from four sectors including electricity, steel, cement, and chemicals accounting for approximately 40 % of global industrial carbon emissions [2]. CO_2 emissions from the cement industry consistently rank among the top three globally. Therefore, reducing CO_2 emissions from the cement industry to achieve green and sustainable development holds significant importance for global energy conservation and emission reduction efforts. However, due to the characteristics of raw materials and production processes, energy conservation and emission reduction in the cement industry are very challenging. Industrial data reveals that producing 1 ton of cement clinker requires the consumption of 113.5 kg of standard coal and results in the emission of 0.8 tons of CO_2 [3]. CO_2 emissions from cement production can be categorized into direct and indirect emissions. Indirect emissions occur during electricity generation and transportation processes, while direct emissions stem from the decomposition of calcium carbonate and the combustion of fossil fuels during the production process. Although it is possible to reduce carbon emissions associated with new concrete construction by extending the life of concrete structures through reinforcement and repair [4–8], finding low-carbon and sustainable alternatives to traditional concrete remains a primary focus and mainstream topic of current research [9–11].

Limestone calcined clay cement (LC^3) is a novel ternary cement based on a mixture of calcined clay and limestone [12]. It utilizes the synergistic effect of calcined clay and limestone to achieve strength development similar to Ordinary Portland Cement (OPC), even when the clinker is as low as 40–50 % [13–18]. Carbon dioxide emissions can be reduced by up to 30 % with LC^3[19,20], which is made from abundantly available limestone and low-grade clay, offering cost-effectiveness without the need for capital-intensive retrofitting of existing cement plants. Following the proposal of LC^3, Scrivener et al.[21], building

* Corresponding author at: Department of Civil Engineering, Chongqing Jiaotong University, Chongqing 400074, PR China.
E-mail address: qiluo@cqjtu.edu.cn (Q. Luo).

https://doi.org/10.1016/j.conbuildmat.2024.137852
Received 3 May 2024; Received in revised form 25 July 2024; Accepted 7 August 2024
Available online 10 August 2024

upon research on the substitution of calcined clay and limestone for cement clinker, proposed the combination of calcined clay, limestone, gypsum, and cement clinker in proportions to form a new type of binder material system, known as LC^3-X, where X represents the mass percentage of cement in the system [22]. The most commonly used composition of the LC^3 system is LC^3-50, comprising 50 % cement, 30 % calcined clay, 15 % limestone, and 5 % gypsum [23].

Research by Vance K. et al. [24] found that incorporating 10 % mass fraction of metakaolin instead of cement can increase the yield stress of cement paste by 77 % and the plastic viscosity by 140 %. Due to the high cost of high-grade calcined clay, Nithya et al. [25] utilized low-grade clay with a lower kaolin content, alongside limestone and clinker, to formulate the LC^3 system, demonstrating the need for increased dosages of high-efficiency water reducers. Chen et al. [26] investigated the impact on the rheological properties of LC^3 mortar by increasing the content of fine particle MK in calcined clay, revealing a significant increase in yield stress values and notable shear thickening behavior with increasing proportions of fine particle MK. Consequently, from a rheological perspective, calcined clay with a coarser particle size and lower MK content appears to be a rational candidate. Muzenda et al. [27] examined the rheological properties of pastes composed of varying amounts of calcined clay and limestone mixtures, indicating significant differences between the rheological properties of the LC^3 system and the OPC system. With an increase in SCM content, the plastic viscosity, static yield stress, dynamic yield stress, cohesion, and adhesion of the paste increased. Globally, the content of metakaolin in clay varies widely; however, there is currently limited research on the impact of metakaolin content in calcined clay on its rheological properties. Given the critical role of rheological characteristics in the engineering application of cementitious materials, gaining a comprehensive understanding of the rheological properties of LC^3 with these specific characteristics is an urgent issue that must be addressed.

To explore the influence of varying metakaolin contents within calcined clays on the rheological property of LC^3, we have developed a novel LC^3 system. Initially, quartz is finely ground to a particle size comparable to that of the calcined metakaolin, and then proportionally mixed with calcined metakaolin to prepare calcined clay blends with full range of metakaolin ratios (from 0 % to 100 %). This method is designed to neutralize the effects of impurities in the clays, thereby providing clearer insights into how metakaolin content specifically influences LC^3 rheological property. The study utilizes rheology tests to measure the flow characteristics of the calcined clay mixtures. Additionally, limestone in the system was replaced with wollastonite to verify the impact of substances with different microstructures (spheroidal and acicular) on the rheological properties of the entire system. Finally, the effects of different w/b and varying amounts of high-range water reducers were also evaluated. This study aims to explore the interaction between metakaolin content and additives such as limestone and wollastonite in the rheological properties of the LC^3 system, ultimately promoting the practical understanding and application of this emerging material technology.

2. Experiments

2.1. Raw materials and mixture design

The study employed OPC with a strength grade of 42.5. The chemical compositions of metakaolin, limestone (wollastonite), and gypsum are presented in Table 1, and the particle size distributions of the raw materials are depicted in Fig. 1. It can be observed from Table 1 that metakaolin, limestone, and gypsum contain high proportions of SiO_2, CaO, and Al_2O_3. The production of ground quartz, as shown in Fig. 1, was conducted using a planetary mixer at a rotational speed of 400 rpm for 1.5 h. This process resulted in a median particle size (D_v50) of 19.33 μm for the ground quartz, which closely matches the particle size of the calcined clay. In this study, the water-to-binder ratio (w/b) is set at 0.5. The ground sand used to replace metakaolin is also considered an active substance and treated as part of the cementitious material.[28, 29]. Additionally, same method [30] was adopted to determine the gypsum content in this experiment, utilizing the heat of hydration method. The heat of hydration curve was observed, ensuring the aluminate peak appeared within 30 h and was clearly distinguishable from the silicate peak. Thus, the optimal gypsum content was determined. Fig. 2 illustrates the microscopic morphology of the raw materials. Various combinations of these materials were mixed to achieve the mix proportions described in Table 2. LC^3-50–85-L was selected to investigate the influence of water-to-binder ratio and dosages of superplasticizer on rheological properties. Five water-to-binder ratio were tested. Concurrently, experiments were conducted on varying dosages of superplasticizer, ranging from 0 to 0.6 wt% of the cementitious material.

2.2. Experimental methods

2.2.1. Rheological test

The rheological properties of LC^3 paste were measured using a rotational rheometer (MCR- 102, Anton Paar). Rheological experiments, including flow curves and stress growth tests, were conducted under room temperature conditions.

2.2.2. Flow curve

The testing scheme for flow curves involves variable-speed shearing from 0 to 100 s^{-1}, with the initial 60 seconds serving as pre-shearing to eliminate the influence of particle agglomeration. Subsequently, the shearing rate is increased to 100 s^{-1}. Rheological parameters are calculated based on the stable portion of the curve after pre-shearing. In general, paste exhibits either shear thinning or shear thickening behavior under shear[31–35]. In this experiment, the paste shows shear thinning behavior, and the Bingham model is employed for curve fitting, as shown in Eq. (1).

$$\tau = \tau_0 + \mu\gamma \quad (1)$$

The equation includes two parameters: yield shear stress and viscosity coefficient, with τ representing shear stress in Pa, τ_0 denoting yield stress in Pa, μ indicating plastic viscosity in Pa·s, and γ representing

Table 1
Chemical composition of raw materials.

wt%	Cement	Metakaolin	Limestone	Gypsum	Wollastonite	Quartz
SiO_2	20.31	54.31	1.25	3.47	50.47	96.2
Al_2O_3	4.40	44.23	0.87	0.51	0.08	0.43
Fe_2O_3	3.7	/	0.44	0.16	0.15	0.92
K_2O	/	< 0.30	0.09	/	/	0.09
CaO	62.58	/	96.44	33.87	45.26	0.09
Na_2O	/	/	0.07	0.10	/	0.04
MgO	3.58	/	0.68	0.10	0.8	0.06
SO_3	3.68	/	0.03	53.96	/	0.03
Loss on ignition (%)	1.94	0.50	/	/	/	/

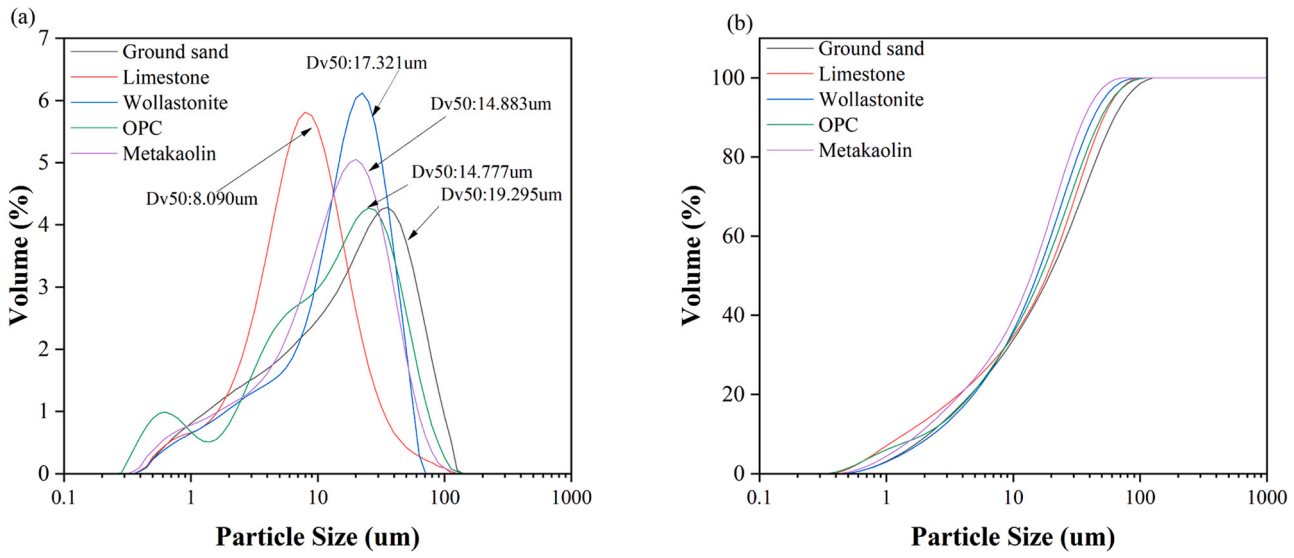

Fig. 1. Particle size distribution of ground quartz.

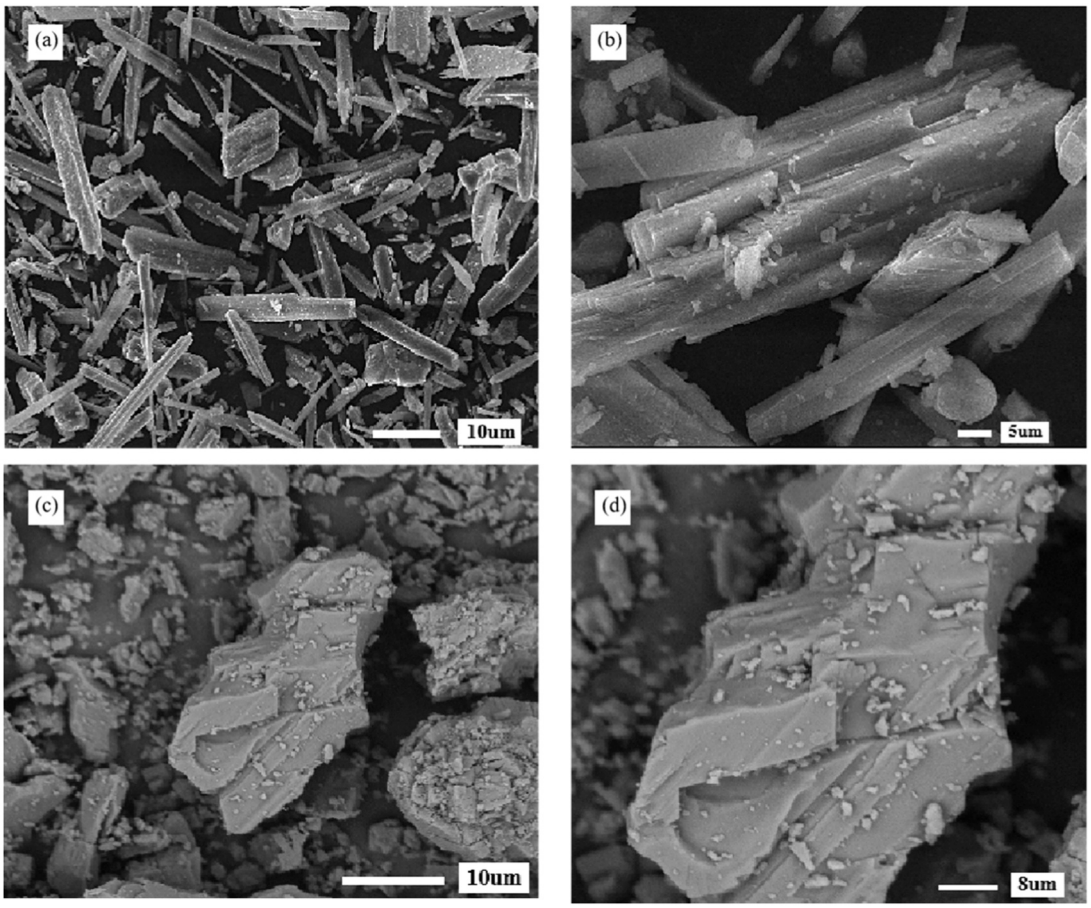

Fig. 2. Microscopic morphology of limestone and wollastonite. (a) and (b) are microstructures of wollastonite, while (c) and (d) are microstructures of limestone.

shear rate in s^{-1}.

2.2.3. Stress growth experiment

Considering the mixing, transfer, and pre-shearing processes, the first stress growth experiment is initiated approximately 5 min after the contact between the binder material and water, referred to as the 5-minute experiment. Subsequently, the specimen is allowed to stand for 10 min, followed by the second stress growth experiment, defined as the 15-minute experiment. This process is repeated till 45 min [36].

2.2.4. Isothermal calorimetry

The hydration process at 3 days was investigated at 20°C using isothermal calorimetry (TAM Air, TA Instruments)[37]. Paste was prepared with a liquid-to-solid weight ratio of 0.5, 75 g of the paste was

Table 2
Mix-design (wt%).

effective constituent	cement	metakaolin	limestone	wollastonite	gypsum	ground quartz
LC3−50–100-L	50	30	15	0	5	/
LC3−50–85-L	50	25.5	15	0	5	4.5
LC3−50–55-L	50	16.5	15	0	5	13.5
LC3−50–25-L	50	7.5	15	0	5	22.5
LC3−50–10-L	50	3	15	0	5	27
LC3−50–0-L	50	/	15	0	5	30
LC3−50–100-W	50	30	0	15	5	/
LC3−50–85-W	50	25.5	0	15	5	4.5
LC3−50–55-W	50	16.5	0	15	5	13.5
LC3−50–25-W	50	7.5	0	15	5	22.5
LC3−50–10-W	50	3	0	15	5	27
LC3−50–0-W	50	/	0	15	5	30

stirred with an electric mixer at 1200 rpm for 2 min, and then 13 g of the paste was transferred into ampoules and placed into the calorimeter.

2.2.5. Compressive strength

According to EN-196–1[38], 40 mm×40 mm×40 mm cubic mortar specimens were cast using a w/b of 0.5. In the LC^3-50 system, polycarboxylate superplasticizers were used (at dosages ranging from 0 to 0.5 wt% of the binder material). The mortar specimens were demolded after 1 day and then cured in water baths for various testing ages. Compression strength measurements were conducted on specimens cured for 1, 7, 14, 28, and 56 days using a loading rate of 2.4 kN/s. The binder is the sum of OPC, metakaolin, limestone, ground sand, and gypsum.

3. Results

3.1. Rheological property

3.1.1. Influence of metakaolin content

The data presented in Fig. 3 suggests a complex relationship between the metakaolin content in LC^3 mortar and its rheological properties, specifically shear stress and apparent viscosity. Contrary to what might be expected, the shear stress does not demonstrate a straightforward linear trend in relation to the metakaolin content. Notably, the LC^3-50–85-L group exhibits a shear stress of 346 Pa, which unexpectedly exceeds that of the LC^3-50–100-L group. This anomaly may be attributed to the agglomerative adsorption properties of metakaolin, indicating that a metakaolin content of 100 % does not necessarily result in optimal rheological behavior; rather, an 85 % content ratio appears to be more influential. This non-linear behavior suggests that there is an ideal balance between metakaolin and impurities—ground quartz in this case—which affects the rheological properties. The ground quartz, with its larger particle size compared to metakaolin, might contribute to a denser particle packing, consequently affecting the flow characteristics of the mortar [39,40]. Overall, the highest shear stress values are observed at metakaolin contents of 85 % (the LC^3-50–85-L has a metakaolin to ground quartz weight ratio of approximately 5.67:1) and 100 %, while intermediate levels of shear stress are seen at 10 %, 25 % (metakaolin to ground quartz weight ratio of 1:3), and 55 % (metakaolin to ground quartz weight ratio of 1.22:1), showing that a near-equal weight presence of metakaolin and ground quartz still provides substantial shear stress. The lowest values are recorded for the 0 % (The suggests that the absence of metakaolin reduces shear stress). These findings propose that the rheological performance of LC^3 mortar is influenced by a dual factor: the content of metakaolin and the presence of impurities. Understanding this balance is crucial for optimizing the material's performance for specific engineering applications. The rheological parameters calculated from curves in different shear rate regions are summarized in Fig. 3 and Table 3.

3.1.2. Influence of different water-to-binder (w/b) ratio

Fig. 4 depicts the influence of different w/b ratios on the rheological properties of LC^3 mortar, demonstrating that as the w/b ratio increases, there is a discernible decrease in both shear stress and apparent viscosity across a range of shear rates. This trend suggests that higher water content in the mortar mix leads to a reduction in the resistance to flow under shear. At the highest w/b ratio of 0.65, the shear stress is significantly lower across all shear rates compared to the lowest w/b ratio of

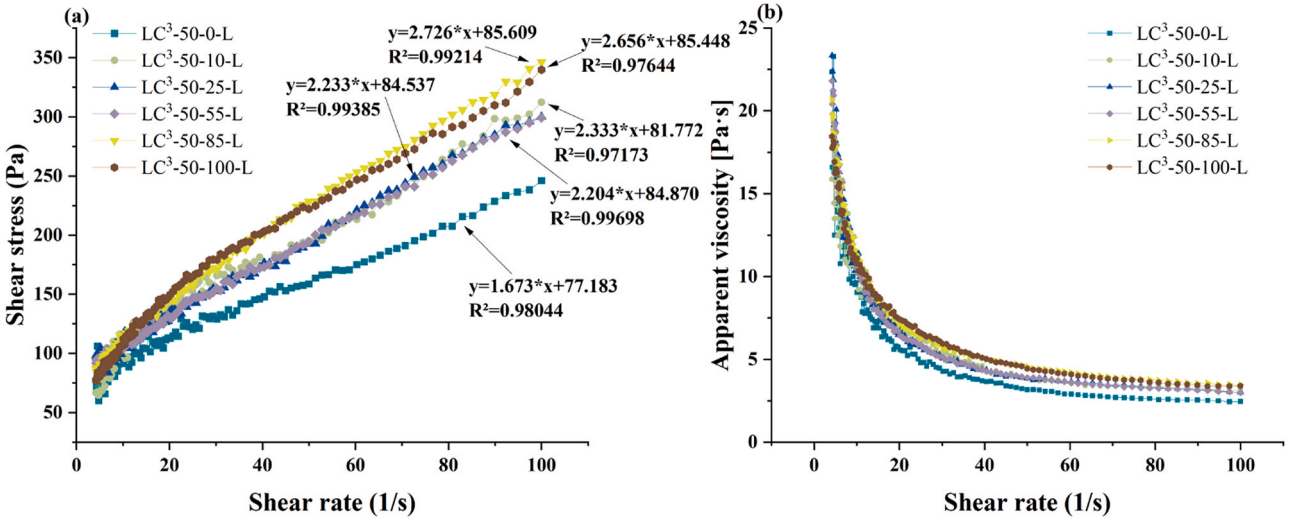

Fig. 3. The influence of different metakaolin content in calcined clay on the shear stress (a) and apparent viscosity (b) of LC^3 mortar.

Table 3
Summary of rheological parameters of LC^3 mortar.

Mix	0–100 s^{-1}		
	τ_0	μ	R^2
LC3−50−100-L	85.448	2.656	0.98
LC3−50−85-L	85.609	2.726	0.99
LC3−50−55-L	84.870	2.204	0.99
LC3−50−25-L	84.537	2.233	0.99
LC3−50−10-L	81.772	2.333	0.97
LC3−50−0-L	77.183	1.673	0.98

0.45, indicating that the mix becomes less cohesive with more water, leading to easier flow. Consistent with the shear stress results, the apparent viscosity (Fig. 4b) also decreases with higher w/b ratios[41]. The mortar with the lowest w/b ratio (0.45) exhibits the highest viscosity, and as the w/b ratio increases, the viscosity decreases, showing a steep drop in the initial shear rate range before leveling off. This reduction in viscosity implies improved workability; however, it may also suggest a potential for segregation at higher w/b ratios. Notably, at a w/b ratio of 0.45, there is an observed increase of 463 Pa in shear stress as the shear rate escalates, underscoring the rigidity of the mix at this ratio. Based on the observations from Fig. 4, it can conclude that the data for a w/b ratio of 0.45 is indeed the most outstanding in terms of higher shear stress and viscosity, the data for a w/b ratio of 0.5 follows, showing a slight reduction in these properties. Furthermore, the differences in rheological properties become less pronounced as the w/b ratio increases beyond 0.5. The changes between the 0.55, 0.6, and 0.65 w/b ratios are not as substantial, suggesting that the influence of the w/b on the rheological performance of LC^3 mortar diminishes after surpassing the 0.5 threshold. This pattern implies that there is a diminishing return on changes in flowability with the addition of water beyond a certain point (w/b 0.5 in this paper). Overall, the data clearly indicates that the w/b ratio is a key determinant of rheological properties in LC^3 mortar.

3.1.3. *Influence of dosages of water reducing agent*

Fig. 5 displays the effects of varying dosages of superplasticizer (Polycarboxylic superplasticizer, PCE) on the rheological properties of LC^3 mortar, as seen in the changes in shear stress Fig. 5(a) and apparent viscosity Fig. 5(b) across different shear rates. The addition of PCE generally leads to a reduction in shear stress and apparent viscosity, indicating an enhanced flowability of the mortar. Without any superplasticizer (0 % dosage), the mortar exhibits the highest shear stress, suggesting a more cohesive and rigid mixture. With an increment to 0.1 % dosage, there is a decrease in shear stress, highlighting the effectiveness of PCEs in reducing internal friction. As the dosage of PCE increases, the decrease in shear stress and apparent viscosity becomes

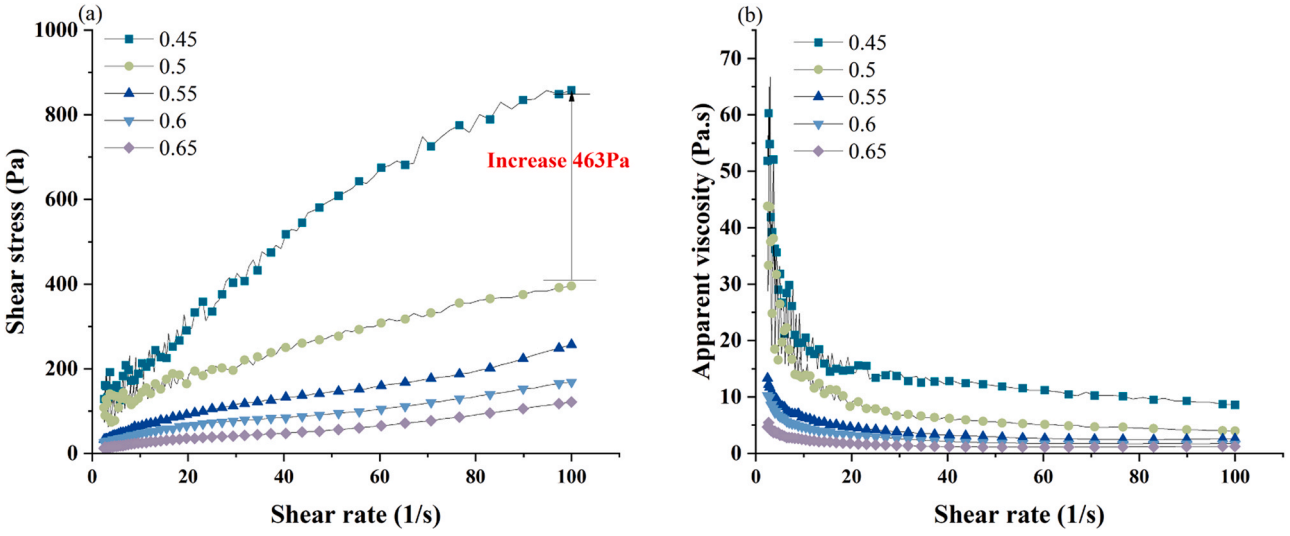

Fig. 4. The influence of different w/b on the rheological properties of LC^3 mortar.

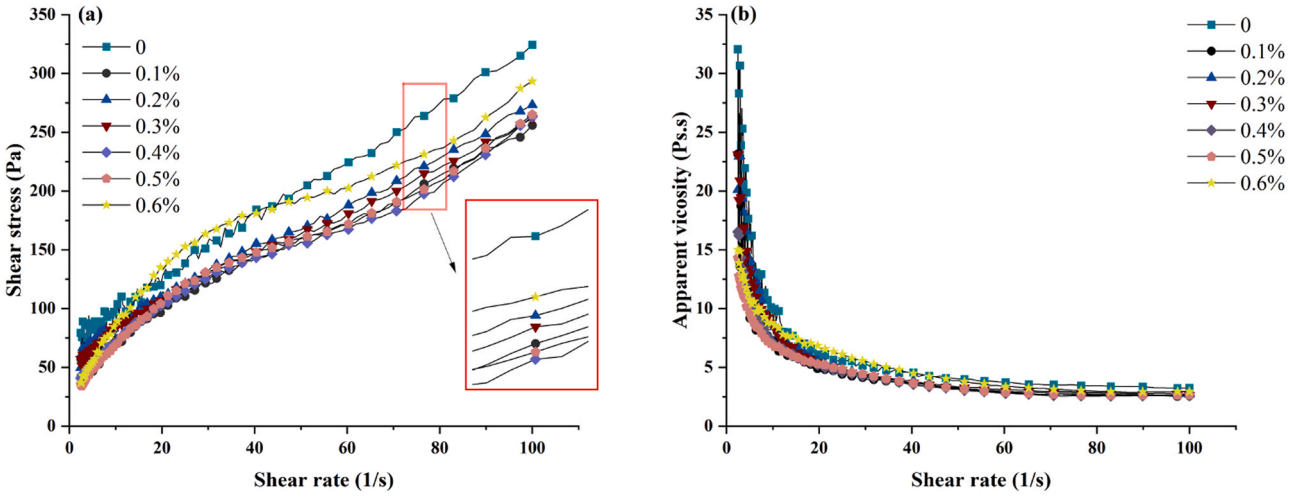

Fig. 5. Effect of water reducing agent dosage on the rheological properties of cement mortar.

less marked, with the groups from 0.2 % to 0.6 % showcasing a plateau in rheological behavior. Particularly, beyond a dosage of 0.5 %, the impact on flowability gains is minimal, echoing the diminishing returns observed with w/b ratios higher than 0.5[42]. The data underscores that while the inclusion of PCE can substantially improve the workability of LC^3 mortar, there is a threshold beyond which additional dosage has a negligible effect on the flow properties[43]. This finding indirectly suggests that PCE-type superplasticizer are not suitable for the LC^3 system.

3.1.4. Influence of resting times

The graph illustrates the influence of different resting times on the rheological properties of the material. It is evident that as the resting time increases, there is a consistent upward trend in shear stress. At the 5-minute mark, the material exhibits the lowest shear stress, implying a more fluid and less resistant mixture immediately following mixing[44,45]. As the resting time extends to 15, 25, 35, and finally 45 min, the shear stress progressively increases, indicating that the material becomes more resistant to shear and, consequently, more cohesive over time. This increment in shear stress with longer resting times suggests that the viscosity of LC^3 mortar is rising due to the ongoing hydration or thixotropic reactions, which are time-dependent. Therefore, the resting time is a critical factor that must be controlled to ensure consistent workability, particularly in the context of construction applications where timing can affect the ease of placement and compaction. Fig. 6

3.1.5. Rheological properties of metakaolin-wollastonite systems

This section explores the rheological behavior of LC^3 mortar systems by substituting limestone with wollastonite, focusing on their microstructural differences, and resulting effects on rheological properties. As shown in Fig. 2, limestone typically exhibits a spheroidal microstructure, which is hypothesized to enhance the flowability of the mortar. In contrast, wollastonite displays acicular, which is speculated not to support flow enhancement within the system. To empirically test this hypothesis, rheological experiments were conducted using two distinct groups within the LC^3 series: LC^3-50–85-L, incorporating limestone, and LC^3-50–85-W, incorporating wollastonite. Fig. 7 illustrates the outcome of these experiments, showing that under identical shear rates, the mortar containing wollastonite (LC^3-50–85-W) exhibited significantly higher maximum shear stress, reaching 425.1 Pa, compared to 324.3 Pa in the limestone-based mortar (LC^3-50–85-L).

This analysis confirms the initial hypothesis: the acicular structure of wollastonite does not promote flowability in the cement system. Instead, it leads to a more viscous mortar, resulting in higher shear resistance and, consequently, increased shear stresses [46]. In contrast, the spheroidal shape of limestone enhances the flowability of LC^3 mortar, acting similarly to a "ball-bearing"[47].This morphology reduces internal friction, allowing components to move more freely, thus facilitating smoother flow, and reducing shear resistance [48,49]. These observations underscore the critical impact of microstructural characteristics of aggregates on the rheological behavior of LC^3 mortar. Understanding these effects is essential for tailoring material compositions to achieve specific rheological properties in various applications.

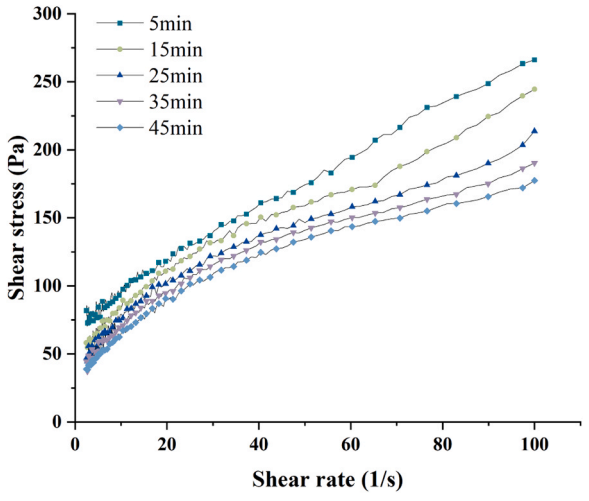

Fig. 6. The stress growth of mortar with LC^3-50–55-L at different curing times.

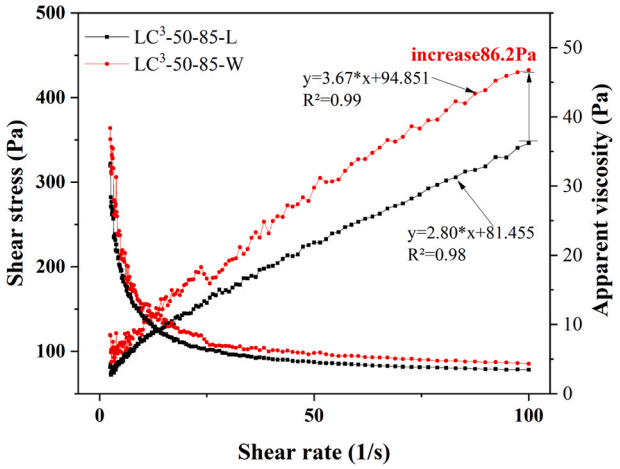

Fig. 7. Comparison of shear stress between adding limestone and wollastonite.

3.2. Hydration and heat release

The hydration behavior of the system was assessed using both the heat release rate and cumulative heat release, as depicted in Fig. 8. The first peak is associated with the hydration of C_3S, and the second with the hydration of aluminates. It was noted that as the metakaolin content decreased, the peak of C_3S hydration shifted rightward, indicating a retardation effect on the early hydration reaction of the LC^3 with more impurify (less metakaolin) [50]. This shift could be attributed to the larger particle size of grounded quartz, which unlike metakaolin, does not provide additional nucleation sites for C-S-H gel formation and offers a greater filling effect [51,52]. Furthermore, grounded quartz extended the induction period, delayed the onset of the C_3S hydration peak, and diminished its intensity. This substitution also reduced the peak value of C_3S hydration, suggesting that grounded quartz adversely affects the hydration process by hindering the hydration reactions[53]. With an increase in grounded quartz content, both the evolution rate and cumulative heat of hydration were observed to decrease. Additionally, the addition of grounded quartz caused the aluminate hydration peak to appear earlier, albeit with reduced intensity.

The cumulative heat release graph indicates that the total heat release diminishes with the reduction of metakaolin content. The lowest heat release is observed when metakaolin is entirely replaced by grounded quartz, as this composition lacks the pozzolanic reactions characteristic of metakaolin.

3.3. Compressive strength

The compressive strength of the blended systems with 50 % metakaolin and limestone replacing 50 % of the cement clinker is shown in Fig. 9, where the compressive data for the six groups exhibit a rising trend with the increase in metakaolin content. The decrease in cement clinker leads to a reduction in hydration products, resulting in lower early compressive strength before 1 day due to the adhesive effect of the cementitious materials. The impact of using ground sand to replace metakaolin on early strength is limited. As hydration progresses, pozzolanic activity becomes particularly significant in the early stages of

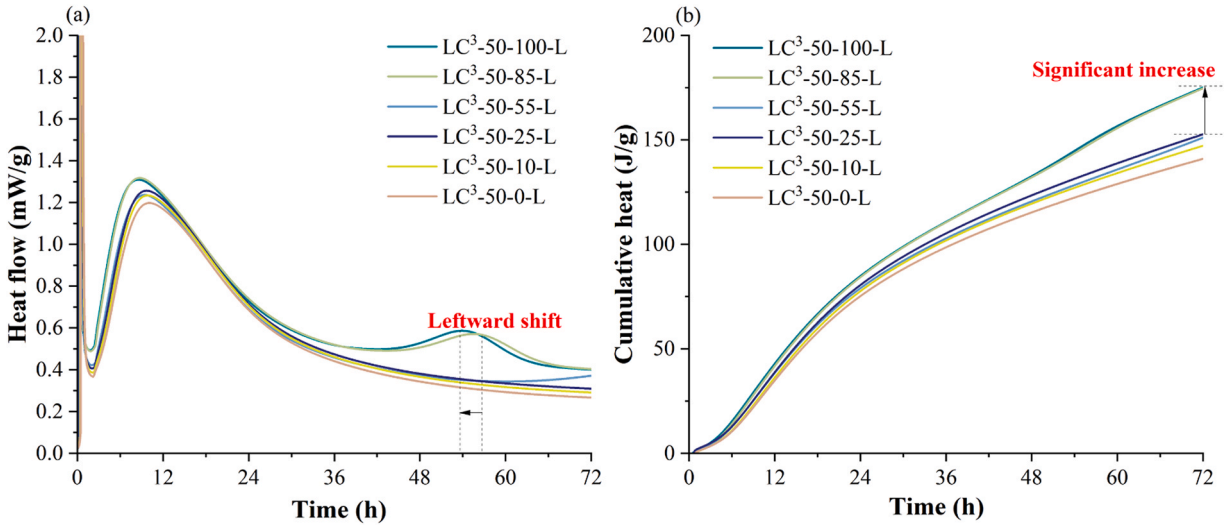

Fig. 8. hydration heat evolution, (a) Heat release rate and, (b) Cumulative heat release.

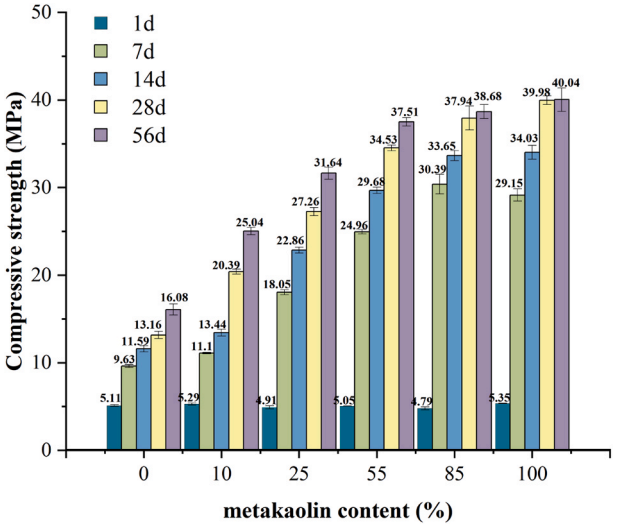

Fig. 9. Compressive strength of different metakaolin contents LC^3 mortar at different ages.

hydration. The early compressive strength from 1 to 7 days increases rapidly, with the LC^3-50–85-L group experiencing the greatest increase up to 25.6 MPa. This increase is attributed to the pozzolanic activity between metakaolin and $Ca(OH)_2$ in the hydration products, resulting in the formation of C-(A)-S-H, which significantly enhances the strength [21,54]. In the blends where ground sand replaces metakaolin, the compressive strength at 7 days shows growth. However, the increase in compressive strength from 14 days to 28 days is lower compared to the increase from 7 days to 14 days, as the $Ca(OH)_2$ in the system reacts with metakaolin and gets consumed[55]. In this study, the XRD test was conducted on samples with an effective component content of 85 % and cured for 7 days, 28 days, and 56 days to verify the results. The XRD patterns are shown in Fig. 10 (a). The patterns shown in the figure were processed to remove the background, and the quantitative results are shown in Fig. 10 (b). The XRD results at different ages indicate that the hydration products include ettringite, calcium hydroxide, and unreacted silicates. As the hydration process progresses, the C_3S content gradually decreases, while the content of formed ettringite remains unchanged. With the increase in curing time, the $Ca(OH)_2$ content gradually decreases. This indicates that metakaolin reacts more with $Ca(OH)_2$ in the later stages of curing, meaning that metakaolin has a significant contribution to the compressive strength in the later stages of curing. During this period, calcined clay does not contribute to strength as it does not undergo pozzolanic activity, thus the development of strength mainly relies on continued hydration of cement, but with a lower content of cement clinker, resulting in lower strength. The graph indicates that while the compressive strength continues to increase during the curing period from 28 days to 56 days, the rate of increase decreases with the increase in metakaolin content. Specifically, the rate of increase in compressive strength from 28 days to 56 days is 22.2 % for the LC^3-50–0-L group, 22.8 % for the LC^3-50–10-L group, 18 % for the LC^3-50–25-L group, 8.6 % for the LC^3-50–55-L group, 1.9 % for the LC^3-50–85-L group, and minimal at 0.1 % for the LC^3-50–100-L group. This suggests that 85 % metakaolin content is the critical threshold for the effective contribution of metakaolin, beyond which not only yields no benefits but also results in material and cost wastage.

4. Discussion

In this study, we investigated the correlation between the rheological properties of various metakaolin content and the hydration heat release. The shear stress data, gathered from rheological experiments conducted at 5, 25, 35, and 45 min after water addition for the LC^3-50–85-L group, were correlated with the corresponding hydration heat release data, as depicted in Fig. 10. The correlation coefficients (R^2) observed in the figure range from a minimum of 0.89 to a maximum of 0.94. Analysis of the experimental data revealed a strong correlation between the rheological properties and hydration heat release of the different effective components. This correlation holds not only theoretical significance but also considerable practical importance. Fig. 11

Currently, the commonly used rheological formulas of cement concrete are as follows: the Newtonian Fluid Model[56], the Bingham Plastic Model[57], the Power Law Model[58], the Herschel-Bulkley Model[59], and the Casson Model[60]. The specific formulas are shown in Eqs. (2) to (6).

$$\tau = \eta\dot{\gamma} \tag{2}$$

$$\tau = \tau_0 + \eta_p\dot{\gamma} \tag{3}$$

$$\tau = K\dot{\gamma}^{\eta} \tag{4}$$

$$\tau = \tau_0 + K\dot{\gamma}^{\eta} \tag{5}$$

$$\tau^{0.5} = \tau_0^{0.5} + (\eta\dot{\gamma})^{0.5} \tag{6}$$

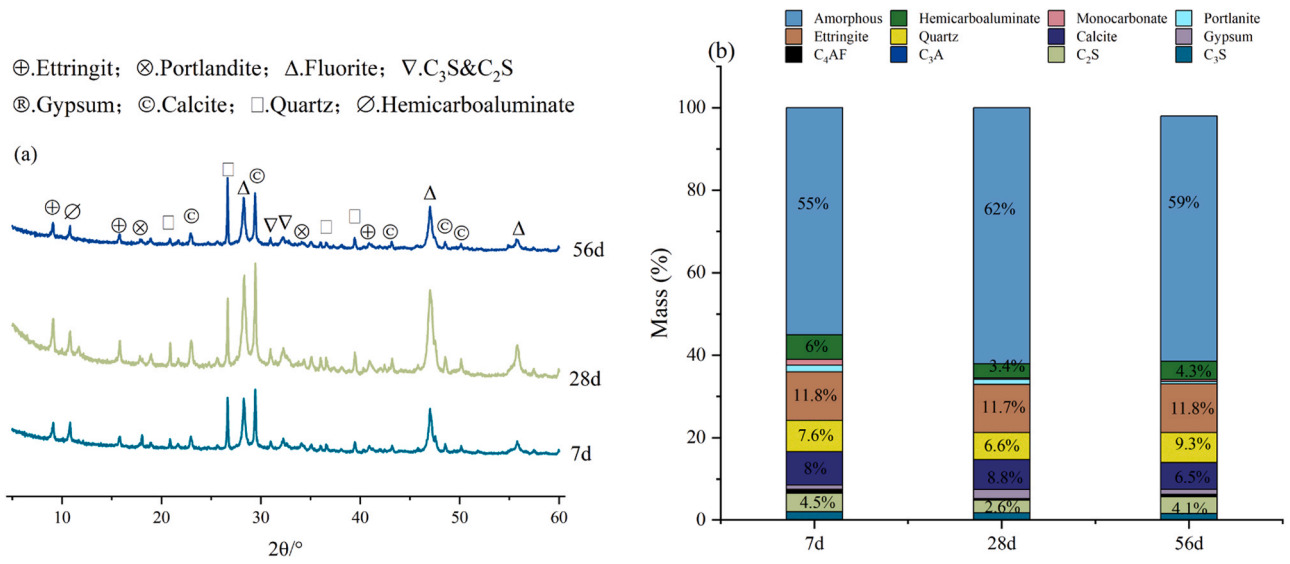

Fig. 10. Analysis results of the samples with 85 % effective component at different curing ages: (a) XRD patterns; (b) QXRD analysis.

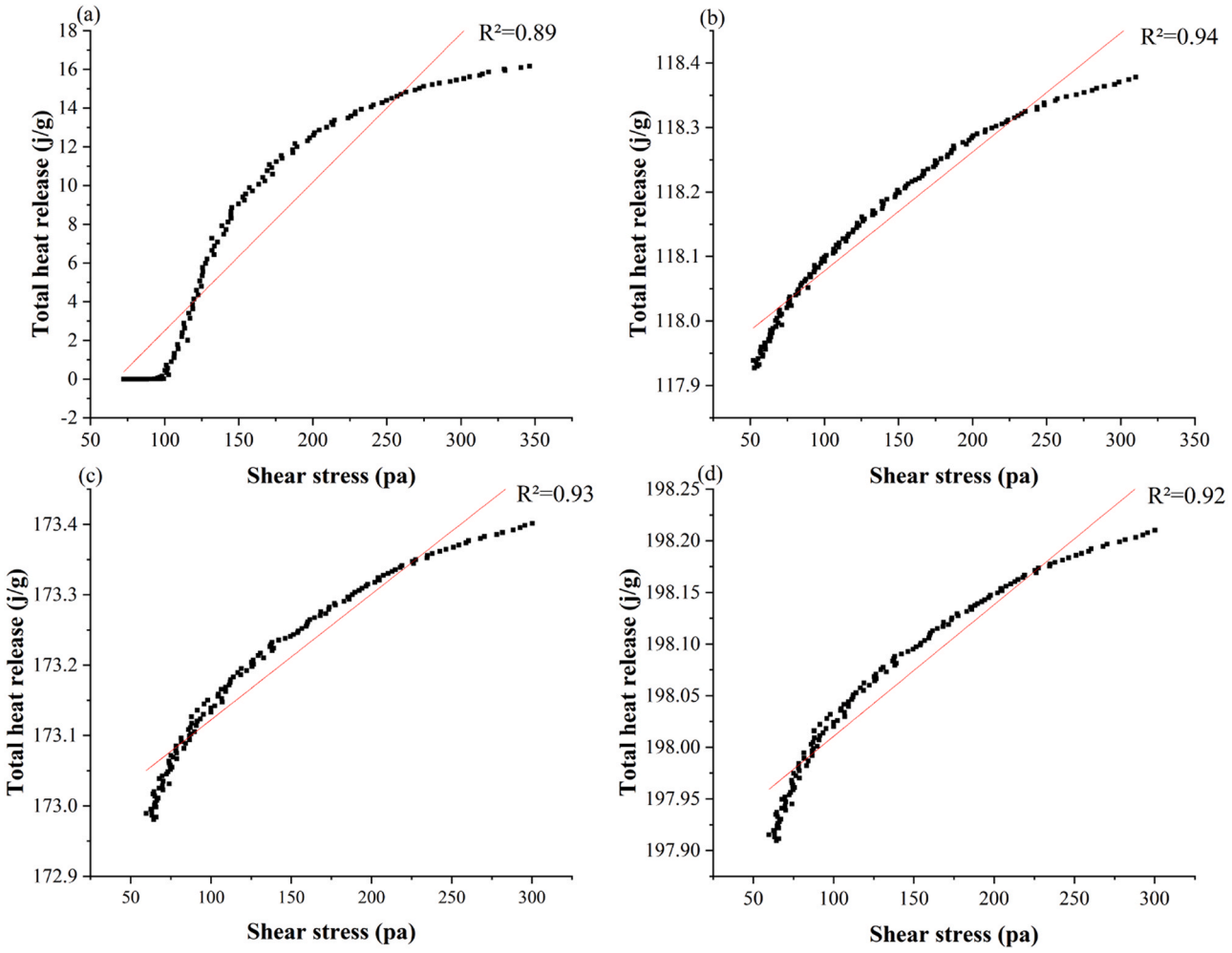

Fig. 11. Correlation between shear stress and hydration heat release, with (a), (b), (c) and (d) stand for 5, 25, 35, and 45 min after water addition for the LC3–50–85-L group, respectively.

However, to the best of our knowledge, there are currently no empirical formulas specifically addressing the rheological behavior of the LC^3 system. Therefore, this study has undertaken some innovations and derivations in this regard. The parameters obtained from the fitting were derived using the least squares method, with the process detailed below.

Error term e_t:

$$e_i = y_i - (ax_i^2 + bx_i + c)$$

The sum of squared errors S is:

$$S = \sum_{i=0}^{n} (y_i - (ax_i^2 + bx_i + c))^2$$

The partial derivatives of S with respect to a, b, and c were calculated, and they were set to zero in order to determine the minimum:

$$\frac{\partial S}{\partial a} = -2\sum_{i=0}^{n} x_i^2 (y_i - ax_i^2 - bx_i - c) = 0$$

$$\frac{\partial S}{\partial b} = -2\sum_{i=0}^{n} x_i (y_i - ax_i^2 - bx_i - c) = 0$$

$$\frac{\partial S}{\partial c} = -2\sum_{i=0}^{n} (y_i - ax_i^2 - bx_i - c) = 0$$

These partial derivatives yield the following linear system of equations:

$$\sum_{i=0}^{n} x_i^4 a + \sum_{i=0}^{n} x_i^3 b + \sum_{i=0}^{n} x_i^2 c = \sum_{i=0}^{n} x_i^2 y_i$$

$$\sum_{i=0}^{n} x_i^3 a + \sum_{i=0}^{n} x_i^2 b + \sum_{i=0}^{n} x_i c = \sum_{i=0}^{n} x_i y_i$$

$$\sum_{i=0}^{n} x_i^2 a + \sum_{i=0}^{n} x_i b + \sum_{i=0}^{n} c = \sum_{i=0}^{n} y_i$$

These equations can be expressed in matrix form AP=Y where:

$$A = \begin{pmatrix} \sum_{i=0}^{n} x_i^4 & \sum_{i=0}^{n} x_i^3 & \sum_{i=0}^{n} x_i^2 \\ \sum_{i=0}^{n} x_i^3 & \sum_{i=0}^{n} x_i^2 & \sum_{i=0}^{n} x_i \\ \sum_{i=0}^{n} x_i^2 & \sum_{i=0}^{n} x_i & n \end{pmatrix}, P = \begin{pmatrix} a \\ b \\ c \end{pmatrix}, Y = \begin{pmatrix} \sum_{i=0}^{n} x_i^2 y_i \\ \sum_{i=0}^{n} x_i y_i \\ \sum_{i=0}^{n} y_i \end{pmatrix}$$

Solving the matrix equation Ap=Y yields the parameters a, b, and c.

As shown in Fig. 12, the six sets of data exhibit a nonlinear relationship. In this study, a unified fitting formula was applied to the rheological data. In processing the data, a quadratic polynomial fit was used, with a goodness of fit (R^2) of 0.93. The final fitted relationship and the obtained results are shown in Fig. 12.

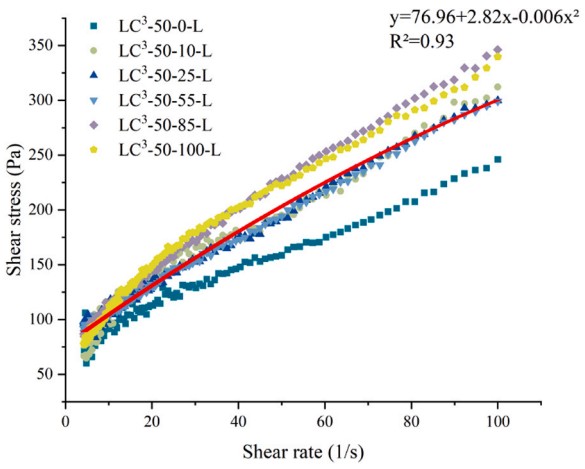

Fig. 12. Rheological data fitting relationship graph.

5. Conclusion

This study developed a novel LC^3 system by finely grinding quartz to a particle size comparable to that of calcined metakaolin and blending it in various proportions to achieve metakaolin ratios ranging from 0 % to 100 %. With this new system in place, we comprehensively investigated the impact of varying metakaolin contents on the rheological properties of LC^3 mortar, using a systematic experimental approach to explore the relationships between metakaolin content, hydration behavior, and both rheological and mechanical properties. From this research, the following conclusions can be drawn:

1) A nonlinear relationship exists between metakaolin content and the rheological properties of LC^3 mortar. Specifically, LC^3-50–85-L, with 85 % metakaolin, shows higher shear stress than LC^3-50–100-L, which contains 100 % metakaolin. The optimal metakaolin content of 85 % is recommended to achieve the best rheological properties in LC^3 mortar.
2) Higher w/b generally reduced shear stress and apparent viscosity, indicating decreased resistance to flow. Moreover, the introduction of wollastonite instead of limestone significantly altered the flow properties due to its needle-like structure, which hindered flowability compared to the ball-bearing effect of spherical limestone particles.
3) Larger particle size and the presence of impurities such as ground quartz affected the hydration kinetics and compressive strength development. Specifically, mixtures with coarser particles and higher impurity levels showed delayed hydration and reduced early strength, which was offset by increased long-term strength development due to ongoing hydration and pozzolanic reactions.

These findings provide crucial insights into optimizing the formulation of LC^3 systems for specific engineering applications, balancing workability, and mechanical strength to achieve desired performance characteristics. In this study, optimization and innovation of the rheological formula for the LC^3 system were carried out, providing insights and conveniences for future research. The relationships among various influencing factors were further refined, and additional variables affecting the performance of LC^3 and similar cementitious systems were explored.

CRediT authorship contribution statement

Qi Luo: Writing – review & editing, Supervision, Methodology, Investigation, Funding acquisition, Formal analysis, Conceptualization. **Jiaqi Zhang:** Writing – original draft, Methodology, Data curation. **Xinyu Zhang:** Writing – review & editing, Data curation, Conceptualization.

Declaration of Competing Interest

The authors declare that they have no known competing financial interests or personal relationships that could have appeared to influence the work reported in this paper.

Data Availability

No data was used for the research described in the article.

Acknowledgements

This study was sponsored by National Natural Science Foundation of China under Grant 52108269, Natural Science Foundation of Chongqing, China under Grant CSTB2022NSCQ-MSX0347, Scientific and Technology Research Program of Chongqing Municipal Education Commission under Grant KJQN202100716 and Team Building Project

for Graduate Tutors in Chongqing (Grant No. JDDSTD2022003).

References

[1] S. O'Neill, Global CO_2 emissions level Off in 2019, with a drop predicted in 2020, Engineering 6 (9) (2020) 958–959.
[2] Bodo Hans, Peter Lungen Dahlmann, Jean-Theo Ghenda, Steel's contribution to a low-carbon Europe 2050: technical and economic analysis of the steel sector's CO_2 abatement potential, Iron Steel Technol. 12 (4) (2015) 62–72.
[3] C. Pang, Analysis and mathematical modeling of factors affecting carbon emissions in the cement industry, South China Univ. Technol. (2012).
[4] Q. Luo, L. Zhao, M. Wu, Microstructural damage characterization of NC-UHPC composite under salt freeze-thaw cycles based on ex-situ X-ray computed tomography, Constr. Build. Mater. 414 (2024).
[5] Q. Luo, X. Zhang, Y. Li, Z. Zhang, G. Geng, Interfacial degradation of calcium silicate hydrate and epoxy under a hygrothermal environment: an experimental and molecular model study, J. Phys. Chem. C 127 (3) (2023) 1607–1621.
[6] Q. Luo, Y. Li, Z. Zhang, X. Peng, G. Geng, Influence of substrate moisture on the interfacial bonding between calcium silicate hydrate and epoxy, Constr. Build. Mater. 320 (2022) 126252.
[7] Q. Luo, T. Qin, Z. Chen, B. Pang, J. Qu, Z. Gao, The influence of moisture and epoxy bonding agents on interfacial behavior between normal concrete substrate and ultrahigh performance concrete as a repair material: experimental and molecular dynamics study, Constr. Build. Mater. 372 (2023).
[8] Y. Xie, Q. Luo, Atomistic insights into the effect of temperature on capillary transport of water molecules in epoxy-modified calcium silicate hydrate nanopore: diffusion, kinetics, and mechanism, J. Mater. Sci. 58 (37) (2023) 14773–14787.
[9] S. Barbhuiya, F. Kanavaris, B.B. Das, M. Idrees, Decarbonising cement and concrete production: strategies, challenges and pathways for sustainable development, J. Build. Eng. 86 (2024).
[10] L. Chen, Z. Huang, W. Pan, R.K.L. Su, Y. Zhong, Y. Zhang, Low carbon concrete for prefabricated modular construction in circular economy: an integrated approach towards sustainability, durability, cost, and mechanical performances, J. Build. Eng. (90 () (2024).
[11] Q. Luo, P. Liu, M. Wu, Re-using excavated rock from underground tunneling activities to develop eco-friendly ultrahigh performance concrete, Case Stud. Constr. Build. Mater. 20 (2024).
[12] K. Scrivener, F. Martirena, S. Bishnoi, S. Maity, Calcined clay limestone cements (LC^3), Cem. Concr. Res. 114 (2018) 49–56.
[13] K. Scrivener, F. Avet, H. Maraghechi, F. Zunino, J. Ston, W. Hanpongpun, A. Favier, Impacting factors and properties of limestone calcined clay cements (LC^3), Green. Mater. 7 (1) (2019) 3–14.
[14] X. Zhang, Y. Bai, Q. Luo, Exploring synergistic effects and hydration mechanisms in metakaolin-blended cement system with varying metakaolin and wollastonite content, Constr. Build. Mater. 425 (2024).
[15] Q. Luo, X. Zhang, Y. Bai, J. Yang, G. Geng, Reduce the cost and embodied carbon of ultrahigh performance concrete using waste clay, Case Stud. Constr. Build. Mater. 19 (2023).
[16] W. Zhang, M. Zhao, Z. Yang, R. Guo, X.Y. Wang, R.S. Lin, Properties of red sandstone-limestone-cement ternary composites: Hydration mechanism, microstructure, and high-temperature damage, Developments in the Built Environment 17 (2024) 100346.
[17] Y. Liao, Y. Lv, G. Huang, S. Ren, X.Y. Wang, R. Guo, R.S. Lin, Strength and microstructure analysis of subgrade materials containing red sandstone-limestone-cement composites and red sandstone gravel, Construction and Building Materials 416 (2024) 135190.
[18] Y. Tian, Q. Luo, Q. Feng, F. Xing, J. Liu, Q. Gu, H. Zhu, Integrated use of Bayer red mud and electrolytic manganese residue in limestone calcined clay cement (LC3) via thermal treatment activation, Journal of Building Engineering 94 (2024) 109974.
[19] M. Sharma, S. Bishnoi, F. Martirena, K. Scrivener, Limestone calcined clay cement and concrete: a state-of-the-art review, Cem. Concr. Res. 149 (2021).
[20] S. Andrea, S. Karen, Limestone calcined clay cement makes inroads in reducing carbon emissions, Concr. Int. 44 (9) (2022).
[21] M. Antoni, J. Rossen, F. Martirena, K. Scrivener, Cement substitution by a combination of metakaolin and limestone, Cem. Concr. Res. 42 (12) (2012) 1579–1589.
[22] K.L. Scrivener, Options for the future of cement, Indian Concr. J. 88 (7) (2014) 11–21.
[23] M.D. Sheikh, T. Jamil, T. Ayub, A.-u-R. Khan, S.M. Bilal, C. Hu, S. Tang, Comparative study on LC^3-50 with OPC concrete using raw materials from Pakistan, Adv. Mater. Sci. Eng. 2023 (2023) 1–10.
[24] K. Vance, A. Kumar, G. Sant, N. Neithalath, The rheological properties of ternary binders containing Portland cement, limestone, and metakaolin or fly ash, Cem. Concr. Res. 52 (2013) 196–207.
[25] N. Nair, K. Mohammed Haneefa, M. Santhanam, R. Gettu, A study on fresh properties of limestone calcined clay blended cementitious systems, Constr. Build. Mater. 254 (2020).
[26] Y. Chen, Y. Zhang, S. He, M. Liang, Y. Zhang, E. Schlangen, O. Çopuroğlu, Rheology control of limestone calcined clay cement pastes by modifying the content of fine-grained metakaolin, J. Sustain. Cem. Based Mater. 12 (9) (2023) 1126–1140.
[27] T.R. Muzenda, P. Hou, S. Kawashima, T. Sui, X. Cheng, The role of limestone and calcined clay on the rheological properties of LC^3, Cem. Concr. Compos. 107 (2020).
[28] F. Avet, K. Scrivener, Investigation of the calcined kaolinite content on the hydration of Limestone calcined clay cement (LC^3), Cem. Concr. Res. 107 (2018) 124–135.
[29] T. Matschei, T.R. Muzenda, F. Georget, Influence of clay impurities on the performance of calcined clay-limestone cements, ce/Pap. 6 (6) (2023) 373–381.
[30] M.R.Cd Silva, Jd.S. Andrade Neto, B. Walkley, A.P. Kirchheim, Exploring sulfate optimization techniques in Limestone calcined clay cements (LC^3): limitations and insights, Cem. Concr. Res. 175 (2024).
[31] D. Feys, R. Verhoeven, G.D. Schutter, Why is fresh self-compacting concrete shear thickening? Cem. Concr. Res. 39 (6) (2009) 510–523.
[32] D. Jiao, C. Shi, Q. Yuan, Time-dependent rheological behavior of cementitious paste under continuous shear mixing, Constr. Build. Mater. 226 (2019) 591–600.
[33] Roussel Nicolas, Lematre Anael, J. Robert, Flatt, Steady, state flow of cement suspensions: a micromechanical state of the art, Cem. Concr. Res. 40 (1) (2010) 77–84.
[34] A.M. Mostafa, P. Diederich, A. Yahia, Effectiveness of rotational shear in dispersing concentrated cement suspensions, J. Sustain. Cem. Based Mater. 4 (3-4) (2015) 205–214.
[35] A. Yahia, Effect of solid concentration and shear rate on shear-thickening response of high-performance cement suspensions, Constr. Build. Mater. 53 (2014) 517–521.
[36] F. Han, Y. Li, D. Jiao, Understanding the rheology and hydration behavior of cement paste with nickel slag, J. Build. Eng. 73 (2023).
[37] E. CEN, 196-8, Methods of Testing Cement–Part 8: Determination of Heat of Hydration–solution Method, CEN, 2005.
[38] S. British, Method of Testing Cement Part1. Determination of strength, (1995).
[39] C.S. Qiang Yuan, Dengwu Jiao, Rheology of Fresh Cement-Based. Materials, CRC Press, 2022.
[40] I. Cerezo-Aizpún, J.F. Velázquez-Navarro, F.J. Rubio-Hernández, Mineral additives geometry influence in cement pastes flow, Adv. Cem. Concr. Res. 23 (2) (2011) 55–60.
[41] M. Harini, G. Shaalini, G. Dhinakaran, Effect of size and type of fine aggregates on flowability of mortar, Ksce. J. Civ. Eng. 16 (1) (2011) 163–168.
[42] Z. Zhang, Q. Feng, W. Zhu, X. Lin, K. Chen, W. Yin, C. Lu, Influence of sand-cement ratio and polycarboxylate superplasticizer on the basic properties of mortar based on water film thickness, Materials 14 (17) (2021).
[43] L.G. Li, A.K.H. Kwan, Roles of superplasticiser dosage, water film thickness and slurry film thickness in flowability of cementitious paste, Adv. Cem. Concr. Res. 29 (7) (2017) 287–301.
[44] Q. Yuan, D. Zhou, K.H. Khayat, D. Feys, C. Shi, On the measurement of evolution of structural build-up of cement paste with time by static yield stress test vs. small amplitude oscillatory shear test, Cem. Concr. Res. 99 (2017) 183–189.
[45] Q. Yuan, D. Zhou, B. Li, H. Huang, C. Shi, Effect of mineral admixtures on the structural build-up of cement paste, Constr. Build. Mater. 160 (2018) 117–126.
[46] W. Li, Z. Huang, F. Cao, Z. Sun, S.P. Shah, Effects of nano-silica and nano-limestone on flowability and mechanical properties of ultra-high-performance concrete matrix, Constr. Build. Mater. 95 (2015) 366–374.
[47] J. Ma, D. Wang, S. Zhao, P. Duan, S. Yang, Influence of particle morphology of ground fly ash on the fluidity and strength of cement paste, Materials 14 (2) (2021).
[48] D.P. Bentz, C.F. Ferraris, S.Z. Jones, D. Lootens, F. Zunino, Limestone and silica powder replacements for cement: early-age performance, Cem. Concr. Compos. 78 (2017) 43–56.
[49] H.S. Yang, K.H. Fang, S.J. Tu, The influence of limestone powder on fluidity, strength and hydration of cement mortar, Adv. Mater. Res. 168-170 (2010) 512–517.
[50] R.I. Khan, W. Ashraf, Effects of ground wollastonite on cement hydration kinetics and strength development, Constr. Build. Mater. 218 (2019) 150–161.
[51] E. Berodier, K. Scrivener, Understanding the filler effect on the nucleation and growth of C-S-H, J. Am. Ceram. Soc. 97 (12) (2015) 3764–3773.
[52] X. Ouyang, D.A. Koleva, G. Ye, K.V. Breuge, Insights into the mechanisms of nucleation and growth of C–S–H on fillers, Mater. Struct. 50 (5) (2017) 213.
[53] G. Liu, Y. Tang, J. Wang, Effects of carbonation degree of semi-dry carbonated converter steel slag on the performance of blended cement mortar – Reactivity, hydration, and strength, J. Build. Eng. (2022).
[54] D.P. Bentz, E.J. Garboczi, Simulation studies of the effects of mineral admixtures on the cement paste-aggregate interfacial zone (SP-105), Acids Mater. J. 88 (5) (1991) 518–529.
[55] T. Abu-Lebdeh, R.V.V. Petrescu, M. Al-Nasra, F.I.T. Petrescu, Effect of nano silica (SiO_2) on the hydration kinetics of cement, Eng. Rev. 39 (3) (2019) 248–260.
[56] I. Peshkov, E. Romenski, A hyperbolic model for viscous Newtonian flows, Contin. Mech. Thermodyn. 28 (1-2) (2014) 85–104.
[57] T.F. Tadros, Fundamental principles of emulsion rheology and their applications, Colloids Surf. A Physicochem. Eng. Asp. 91 (93) (1994) 39–55.
[58] D.M. Wei, S. Al-Ashhab, Similarity solutions for non-Newtonian power-law fluid flow, Appl. Math. Mech. 35 (9) (2014) 1155–1166.
[59] P. Saramito, A new elastoviscoplastic model based on the Herschel–Bulkley viscoplastic model, J. Non-Newton. Fluid Mech. 158 (1-3) (2009) 154–161.
[60] M. Nazeer, F. Hussain, M.K. Hameed, M.I. Khan, Q.H. Shi, Development of mathematical modeling of multi-phase flow of Casson rheological fluid: theoretical approach, Chaos Solitons Fractals 150 (11) (2021) 111198.